Journal of The Electrochemical Society, **157** (11) B1740-B1745 (2010)
0013-4651/2010/157(11)/B1740/6/$28.00 © The Electrochemical Society

Carbon-Supported Palladium–Polypyrrole Nanocomposite for Oxygen Reduction and Its Tolerance to Methanol

C. Jeyabharathi, P. Venkateshkumar,[a] J. Mathiyarasu,[z] and K. L. N. Phani*

Electrodics and Electrocatalysis Division, CSIR-Central Electrochemical Research Institute, Karaikudi 630 006, India

Carbon-supported palladium–polypyrrole (Pd–PPy/C) nanocomposite was synthesized by oxidative polymerization of pyrrole and reduction of palladium(II) precursor salt in the presence of Vulcan XC-72R. The Pd–PPy/C composites were characterized by X-ray diffraction (XRD), Fourier transform IR, X-ray photoelectron spectroscopy (XPS), thermogravimetric analysis (TGA), and transmission electron microscopy (TEM) techniques. The XRD analysis of Pd–PPy/C shows the formation of the face-centered cubic structure of Pd particles and the mean particle size calculated from TEM was 5.3 ± 2.0 nm. The electrochemical stability of Pd–PPy/C was examined by cyclic voltammetry in an acid solution. The thermal stability and Pd loading in the composite was assessed using TGA. The introduction of Pd in the conducting PPy/C matrix gives better catalytic activity toward oxygen reduction with resistance to methanol oxidation. This was further elucidated by the XPS analysis showing d-band vacancy that is attributed to metal–polymer interaction. From the polarization studies, it is observed that even in the presence of methanol there is no significant cathodic shift in the half-wave potential, revealing that Pd–PPy/C is tolerant to methanol. Rotating ring disk electrode studies show that there is only a negligible quantity of hydrogen peroxide produced in the potential region where its production is expected to be high. This confirms that Pd–PPy/C catalyzes reduction of oxygen directly to water through a four-electron pathway.
© 2010 The Electrochemical Society. [DOI: 10.1149/1.3489266] All rights reserved.

Manuscript submitted March 25, 2010; revised manuscript received June 14, 2010. Published September 29, 2010.

Methanol crossover from anode to cathode poses a big challenge for the development of direct methanol fuel cells (DMFCs) because it produces a mixed potential and reduces cell performance. To circumvent this problem, considerable effort has been invested in finding novel methanol-tolerant cathode catalysts with good stability and catalytic activity for oxygen reduction. In state-of-the-art DMFCs, (a) chevral-phase-type compounds,[1,2] (b) N_4 macrocyclic complexes,[3-5] (c) bimetallic platinum and palladium based alloys involving transition metals and p-block metals,[6-13] and (d) trimetallic alloys[14,15] are reported as DMFC cathode catalysts that show methanol tolerance. In one or the other ways, these catalysts are successful to some extent in achieving the required performance. The synthesis of methanol-tolerant cathode materials with high oxygen reduction activity and stability in fuel cell operating conditions is a challenge to the commercialization of DMFCs.[16] A variety of polymer–metal systems[17-20] involving polymers such as polyaniline, polypyrrole, poly(3,4-ethylenedioxythiophene), etc., and metals such as Pt, Pd, Au, etc., are known for chemical and electrocatalytic applications. Mimicking metal–porphyrin complexes using heterocyclic polymer–metal composites is one of the novel ways of finding metal–N sites, which are known for the oxygen reduction reaction (ORR) catalytic activity.[21,22] Recently, Bashyam and Zelenay[23] synthesized carbon-supported cobalt–polypyrrole composites and found the cell performance of this composite material to be very stable with no appreciable drop over 100 h of fuel cell operation. Nitrogen-doped carbon-based catalysts have also been reported as attractive and potential Pt-free electrocatalysts for ORR in polymer electrolyte fuel cells.[24]

Among the transition metals, Pd is a well-known catalyst in many organic reactions[25] and even for ORR.[26] Keeping this in mind, we synthesized carbon-supported palladium–polypyrrole (Pd–PPy/C) with 40% metal loading in a PPy/C matrix with anticipation that Pd forms complexes with polypyrrole, mimicking those of metalloporphyrins.[27] One of the first papers on reducing the influence of methanol on the cathodic reaction examined the effectiveness of a thin coating of palladium on the Nafion membrane in the fuel cell.[28] Electrocatalytic activity toward oxygen reduction in the presence and absence of methanol are evaluated for Pd–PPy/C. In what follows, we show greater reactivity of Pd–PPy/C toward ORR and immunity toward methanol oxidation even at higher concentrations.

Materials and Methods

All chemicals used were of analytical grade. $PdCl_2 \cdot 2H_2O$, (Merck) was used as a metal precursor. Other chemicals used were Vulcan XC-72R, glacial acetic acid (Merck), pyrrole (Lancaster), and sodium borohydride (Merck). All solutions were prepared with ultrapure water (Milli-Q, Millipore).

Synthesis of Pd–PPy/C.— Pd–PPy/C was prepared with a metal loading of 40% in a PPy loaded Vulcan XC 72 (PPy/C). At first, PPy/C was prepared by dispersing 2 g of Vulcan XC 72 in 0.5 mL of glacial acetic acid. 15 mL of water was added to the carbon dispersion and mixed well. 0.415 mL of freshly distilled pyrrole was added and stirred for a few minutes followed by the addition of 2 mL of 10% hydrogen peroxide, the oxidant. This mixture was stirred well for 1 h. The resultant mixture was kept aside for an hour and filtered, washed with warm water, and then dried in a vacuum oven overnight at 90°C. 0.125 g of PPy/C was mixed with 10 mL of ultrapure water (Milli-Q, Millipore). This was heated under refluxing for 30 min with constant stirring. Then, 8.4 mL of 1% palladium chloride solution was added and heated at 75–80°C with vigorous stirring for 30 min. This was followed by the addition of sodium borohydride in sodium hydroxide until the pH is >10. Then, the catalyst powder is filtered, washed with warm water, and then dried in a vacuum oven overnight at 90°C. The above procedure was adopted for the synthesis of the Pd/C catalyst with 40% metal loading in Vulcan XC72 and 40% commercial Pt/C (E-TEK) of ~5 nm in size was used for comparison.

X-ray diffraction.— X-ray diffraction (XRD) measurements of Pd–PPy/C catalysts were carried out on a Philips PANanalytical X-ray diffractometer using Cu Kα radiation (λ = 0.15406 nm). The XRD patterns were obtained in the step-scanning mode with a narrow receiving slit (0.5°) with a counting time of 15 s/0.1°. Scans were recorded in the 2θ range of 15–90°. The identification of the phases was made by referring to the Joint Committee on Powder Diffraction Standards International Center for Diffraction Data database.

Transmission electron microscopy.— Transmission electron microscopy (TEM) analysis was performed using a transmission electron microscope (JEOL, JEM 3010, URP) operating at 300 kV and

* Electrochemical Society Active Member.
[a] Present address: Department of Chemical and Biological Engineering, Illinois Institute of Technology, IL, USA.
[z] E-mail: al_mathi@yahoo.com

Downloaded 19 Jan 2011 to 210.212.252.226. Redistribution subject to ECS license or copyright; see http://www.ecsdl.org/terms_use.jsp

having a resolution of 0.17 nm. The samples for TEM characterization were prepared as follows: A carbon film was deposited onto a mica sheet that was placed onto the Cu grids (300 mesh and 3 mm diameter). The material to be examined was dispersed in water by sonication, placed onto the carbon film and, then left to dry. The average particle size was calculated using about 300 particles.

FTIR spectra.— The Fourier transform infrared (FTIR) spectra were recorded with a Thermo-Electron Corp. Nexus 670 model FTIR spectrometer (DTGS detector). The samples were prepared by mixing the catalyst with KBr powder and pressing the mixture into a pellet. Scans were recorded between 4000 and 400 cm^{-1} (resolution: 4 cm^{-1}).

X-ray photoelectron spectroscopy.— The X-ray photoelectron spectroscopy (XPS) studies were done by using a VG ESCA MK200X instrument. Mg Kα X-ray (1253.6 eV) with 300 W power was used as the exciting source and a pass energy of 10 eV was used for data collection. The energy analyzer employed was a hemispherical analyzer of 150 mm diameter and 1.2×10^{-9} mbar of pressure was maintained during the experiment.

Thermogravimetric analysis.— The thermal stability of PPy/C and Pd–PPy/C samples was analyzed through SDT Q600 V8.3 Build 101 (Universal V4.3A TA Instruments) with a heating rate of 5°C/min in the range from 0 to 800°C under air atmosphere.

Electrochemical characterization.— Preliminary evaluation of the activity of Pd–PPy/C catalysts for the ORR was performed with a half-cell configuration based on linear scan voltammetry (LSV). 10 mg of the catalyst substance, 0.5 mL of Nafion solution (5 wt %, Aldrich), and 2.5 mL of water were mixed under sonication. A measured volume (3 or 10 μL) of this ink was transferred using a syringe onto a freshly polished glassy carbon disk (3 or 6 mm in diameter).

After the solvent evaporated overnight at room temperature, the prepared electrode served as the working electrode. Electrochemical measurements were performed using an Autolab PGSTAT 30 potentiostat/galvanostat [for rotating ring disk electrode (RRDE) experiments, the equipment was coupled to a bipotentiostat module] and a conventional three-electrode electrochemical cell. The counter electrode was a platinum foil and a mercury/mercurous sulfate electrode served as the reference electrode. However, all potentials were referred to the normal hydrogen electrode (NHE). The electrolyte used for half-cell measurements was 0.5 M H_2SO_4 + 0.5 M CH_3OH. The porous electrodes were cycled at a scan rate of 50 mV s^{-1} between 0.03 and 1.2 V vs NHE until reproducible cyclic voltammograms were obtained before any LSV measurements. The electrochemical activity for the ORR was measured with the RRDE technique using an interchangeable ring disk electrode setup coupled with a rotation controller (Pine Instruments). High purity nitrogen and oxygen were used for deaeration and oxygenation of the solutions, respectively. During the measurements, a blanket of nitrogen or oxygen was maintained above the electrolyte surface. Unless stated otherwise, all half-cell tests were performed at a temperature of 25 ± 1°C.

Results and Discussion

Physical characterization of Pd–PPy/C.— Figure 1 shows the XRD patterns of carbon-supported PPy and palladium-incorporated PPy matrices. As expected, the pattern corresponding to PPy–carbon does not yield any characteristic reflections, except the low angle one at ~25° indicating the amorphous carbon material. The reflections observed for Pd–PPy–carbon at (111), (200), (220), and (311) correspond to the face-centered cubic (fcc) structure of crystalline Pd^0 in Pd–PPy/C. The peaks appear to be broader in nature, indicating smaller crystallites. Figure 2 shows the TEM images of the Pd–PPy/C catalyst materials and the corresponding particle size distribution histogram (inset) based on the observation of more than 300 nanoparticles. As can be seen, the present synthetic method did not result in Pd nanoparticles of uniform particle size. However, the spherical nanoparticles are well dispersed on the surface of the polymer–carbon support and the mean particle size is ~5.3 ± 2.0 nm in diameter.

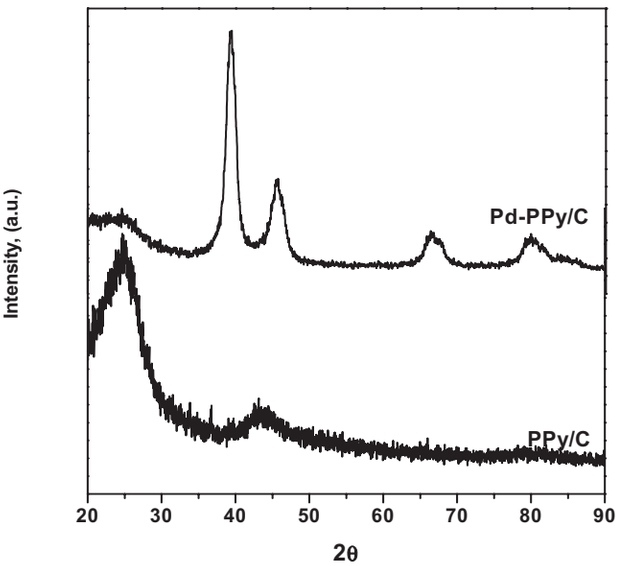

Figure 1. Powder XRD patterns of PPy/C and Pd–PPy/C.

Figure 3 shows the FTIR transmittance spectrum of PPy/C and Pd–PPy/C recorded from 4000 to 400 cm^{-1}. In the FTIR spectrum of PPy/C, the band at 3434 cm^{-1} is attributed to the N–H stretch vibration and a couple of bands at 2921 and 2856 cm^{-1} are assigned to the C–H stretching vibration. The main band at 1630 cm^{-1} is due to the pyrrole ring vibration. The band at 1045 cm^{-1} corresponds to the ═C–H in-plane vibration. The band at 1385 cm^{-1} is due to the N═C stretching vibration.

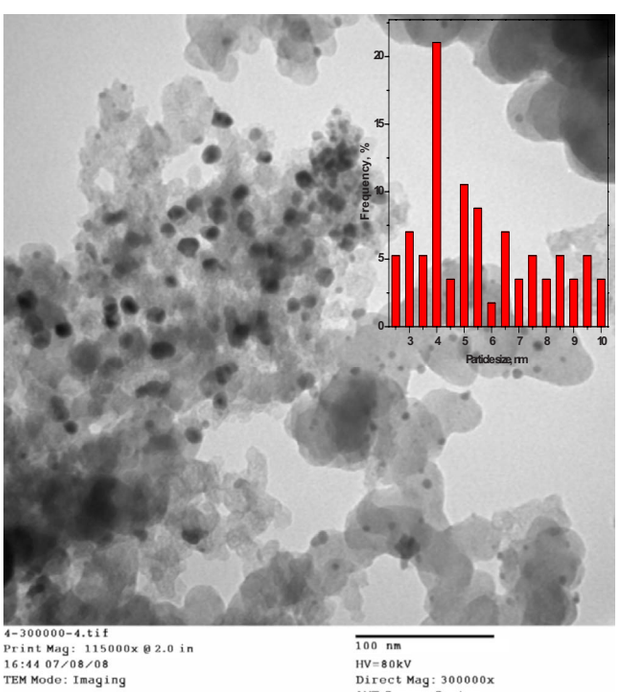

Figure 2. (Color online) TEM images of Pd–PPy.

Downloaded 19 Jan 2011 to 210.212.252.226. Redistribution subject to ECS license or copyright; see http://www.ecsdl.org/terms_use.jsp

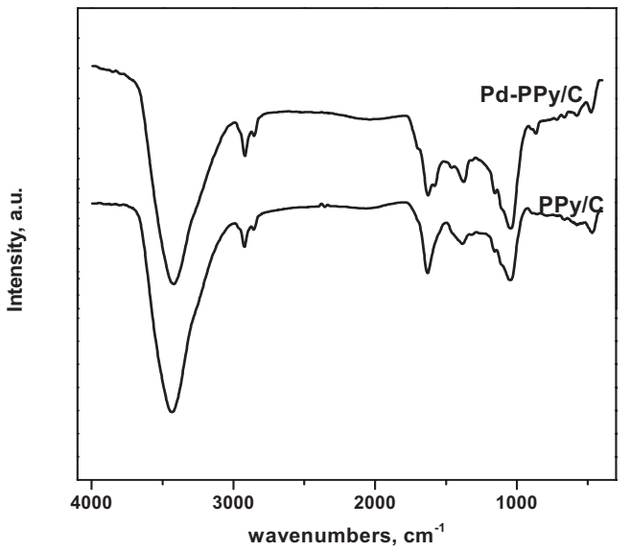

Figure 3. FTIR spectrum of (a) PPy/C and (b) Pd–PPy/C.

Figure 4 shows the XPS analysis of (a) N 1s and (b) Pd 3d in Pd–PPy/C. The Pd 3d core-level photoemission spectra were recorded using the Mg Kα (1253.6.eV) source. Experimental data were curve-fitted with a Gaussian and Lorentzian mix-product function after subtracting the Shirley background. The binding energies of 340.63 and 335.24 eV correspond to the 3d3/2 and 3d5/2 levels of Pd^0, respectively. It is observed from the figure that there is a new peak emerging at 341.5 eV corresponding to 3d3/2, which is 0.87 eV higher than that of Pd^0. In addition to this, there is an additional peak for unreduced palladium at 343.24 and 337.82 eV corresponding to the 3d3/2 and 3d5/2 levels, respectively. The emergence of new peaks at higher binding energy[29] suggests that there is a charge transfer from the metal-to-polymer matrix. The analysis further reveals that 29.44% of Pd^0 is influenced by the donor–acceptor interaction; 56.40% of Pd^0 is unaffected by this interaction and the remaining 14.16% is unreduced Pd. The binding energy at 399.63 eV in the N 1s spectra corresponds to nitrogen in polypyrrole and the new peak at 398.39 eV is attributed to nitrogen interacting with metal through charge transfer, which is 1.24 eV lower than that of nitrogen that is unaffected by such interactions in polypyrrole. Thus, it is realized that the charge transfer is favored from the metal to the polymer. Also, ~30% of nitrogen is under the influence of charge transfer due to metal–polymer interaction. Hence, the charge transfer from Pd to PPy decreases the electron cloud in Pd, thereby increasing the binding energy of electrons in the metal. This is evidenced by the emergence of a new peak at the higher binding energy side of the Pd 3d spectrum. Meanwhile, the electron density of PPy increases as the charge is driven to the polymer from the metal, causing the additional signal at the lower binding energy side of the N 1s spectrum.[29] It is also expected that the decrease in charge cloud in the metal site creates the d-band vacancy that could favor the ORR.[29]

Figure 5 shows the thermogram of PPy/C and Pd–PPy/C samples recorded in the temperature range of 0–800°C at a rate of 5°C/min in air. The oxidative decomposition of PPy/C occurs at 538°C, whereas Pd–PPy/C decomposes at 506°C. The thermal decomposition of Pd–PPy/C is activated in the presence of palladium[23] and the thermal stability of PPy/C is higher than that of Pd–PPy/C. PPy/C decomposes completely, leaving some 2% residue. In the Pd–PPy/C composite, only ~60% of the sample is decomposed, indicating that nearly 40% remains as residue that corresponds exactly to the Pd content in the Pd–PPy/C matrix.

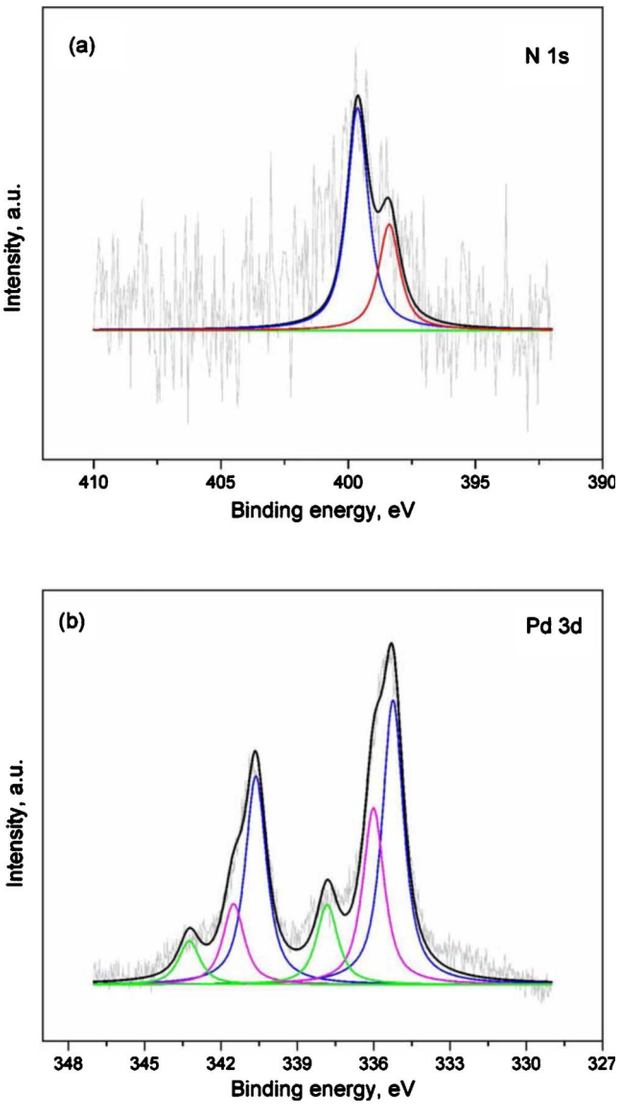

Figure 4. (Color online) XPS spectrum of (a) N 1s and (b) Pd 3d of Pd–PPy/C.

Cyclic voltammetric studies.— Figure 6 shows the cyclic voltammetric behavior of the PPy/C and Pd–PPy/C modified electrode surfaces in 0.5 M sulfuric acid electrolyte. The surface oxidation of Pd to PdO starts at ~0.75 V in the forward scan. The reduction peak at ~0.68 V corresponds to the re-reduction of PdO in the reverse scan of the cyclic voltammogram. In the region of $0 > x < 0.35$ V, a well-defined hydrogen adsorption/desorption is observed. Potential cycling of the catalyst from 0.03 to 1.3 V vs NHE for 25 consecutive runs shows that there is no significant change in the voltammogram of the 1st and 25th cycles (figures not shown). This suggests that the catalyst is very stable under the fuel cell reaction condition.

ORR activity Pd–PPy/C catalyst.— To study the electrocatalytic activity and kinetics of ORR on the Pd–PPy/C catalyst, RRDE experiments were performed in oxygen-saturated 0.5 M sulfuric acid solutions in a potential range from 0.1 to 1 V vs NHE at a scan rate of 5 mV s^{-1} at different rotation rates. Figure 7 shows the comparison of polarization curves for ORR on Pt/C 40% (E-TEK), PPy/C, Pd–PPy/C, and Pd/C in oxygen-saturated 0.5 M sulfuric acid at 1600 rpm. The half-wave potential ($E_{1/2}$) values of ORR at 1600 rpm are

Downloaded 19 Jan 2011 to 210.212.252.226. Redistribution subject to ECS license or copyright; see http://www.ecsdl.org/terms_use.jsp

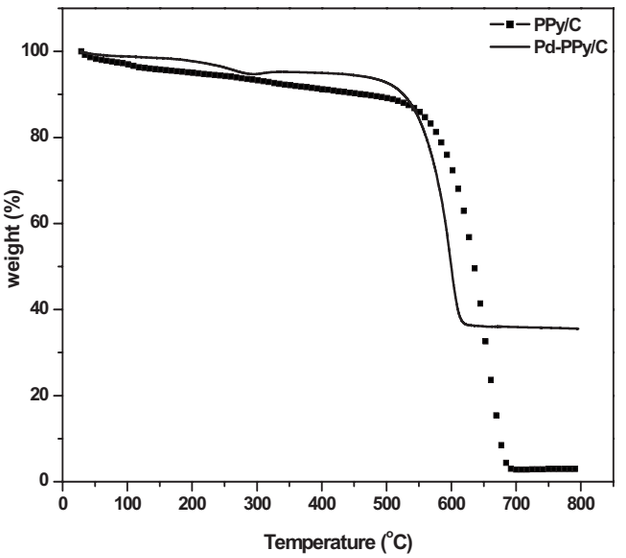

Figure 5. Thermogravimetric analysis of PPy/C and Pd–PPy/C in the temperature range of 0–800°C at the rate of 5°C/min in air.

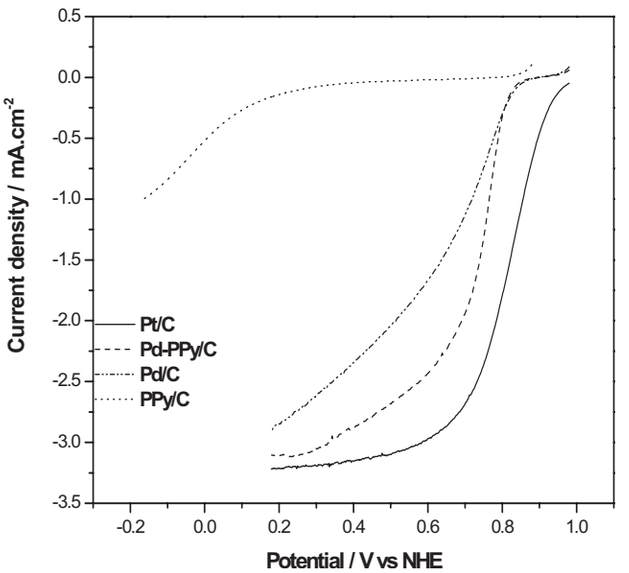

Figure 7. Comparison of polarization curves for the ORR on different catalysts in oxygen-saturated 0.5 M sulfuric acid at 1600 rpm.

0.755 and 0.815 V vs NHE for Pd–PPy/C and Pt/C, respectively, and there is a cathodic shift of ~60 mV in the $E_{1/2}$ value for Pd–PPy/C with reference to that of Pt/C. Based on the position of the half-wave potential, Pd–PPy/C is more catalytically active toward oxygen reduction than Pd/C.

Methanol tolerance of the Pd–PPy/C.— The effect of the presence of methanol on the ORR on Pd–PPy/C catalysts was studied by using 0.5 M methanol in 0.5 M sulfuric acid in the hydrodynamic voltammetric experiments at 1600 rpm at a scan rate of 5 mV s^{-1}. In the presence of methanol, the $E_{1/2}$ of ORR on the Pd–PPy/C catalyst is not affected significantly (Fig. 8) but this is not the case with Pt/C where a shift to the extent of >200 mV is observed. The ORR current on Pd–PPy/C with and without methanol also remains unaffected. This suggests that Pd–PPy/C catalysts show very good methanol tolerance. Independent experiments on methanol oxidation reaction (MOR) on these catalysts indicated the total absence of MOR activity. It can now be recalled from Ref. 28 that palladium in contact with acid solutions under electrochemical conditions can exist as "palladium hydride," which can block methanol from permeating or reacting.

Figure 9 shows the RRDE measurements of oxygen reduction obtained with a ring disk electrode with surface area values of 0.286 and 0.126 cm^2 on Pd–PPy/C in an oxygen-saturated 0.5 M sulfuric acid medium at a scan rate of 5 mV s^{-1} and different rotation rates. The catalytic current density (i) and the kinetic current density (i_k) are related by the Koutecky–Levich (K-L) equation[30]

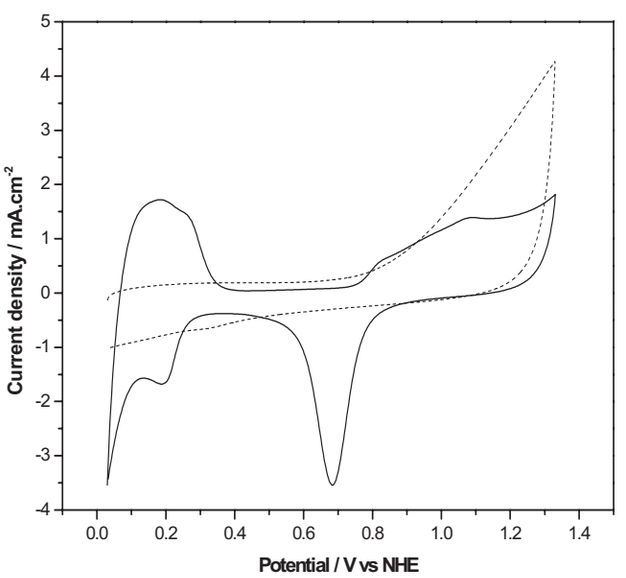

Figure 6. Cyclic voltammogram of PPy/C (dashed line) and Pd–PPy/C (solid line) in 0.5 M sulfuric acid; scan rate: 100 mV s^{-1}.

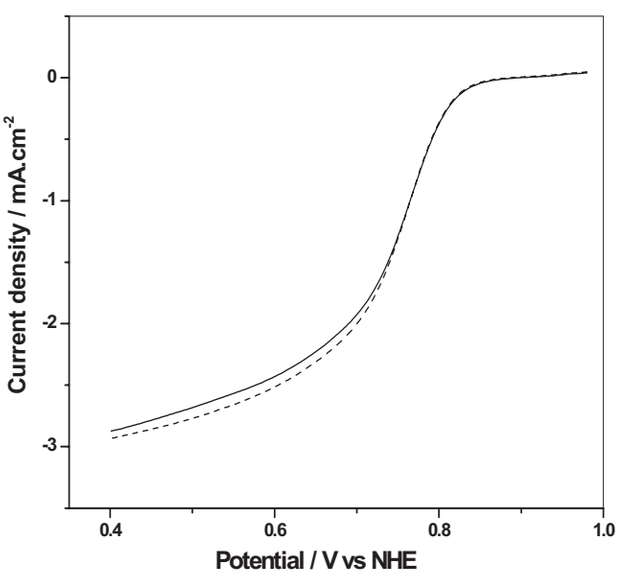

Figure 8. Comparison of polarization curves for ORR on Pd–PPy/C in oxygen-saturated 0.5 M sulfuric acid with (solid line) and without (dashed line) 0.5 M methanol at 1600 rpm.

Downloaded 19 Jan 2011 to 210.212.252.226. Redistribution subject to ECS license or copyright; see http://www.ecsdl.org/terms_use.jsp

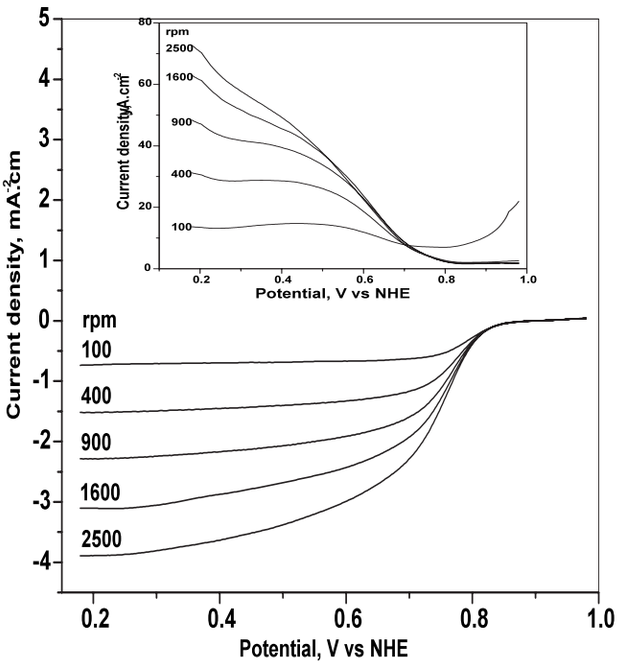

Figure 9. Polarization curves of ORR on Pd–PPy/C catalyst in oxygen-saturated 0.5 M sulfuric acid with different rotation rates indicated in figure; scan rate: 5 mV s^{-1} (inset A is respective ring current at 1.27 V vs NHE).

$$\frac{1}{i} = \frac{1}{i_k} + \frac{1}{i_d} = \frac{1}{i_k} + \frac{1}{0.2nFD_o^{2/3}\omega^{1/2}\nu^{-1/6}C_o} = \frac{1}{i_k} + \frac{1}{B\omega^{1/2}}$$

where i_k is the kinetic current density, B is the Levich slope, n is the number of electrons involved in the ORR per oxygen molecule, C is the saturation concentration for oxygen in the electrolyte (1.1×10^{-6} mol L^{-1}), D is the diffusion coefficient (1.9×10^{-5} cm^2 s^{-1}), ν is the kinematic viscosity of the solution (1.0×10^{-2} cm^2 s^{-1}),[31] and ω is the rotation rate in rpm. The number of electrons involved in the ORR was calculated using the K-L equation, which relates the current density (i) to the rotation rate of the electrode (ω). A plot of i^{-1} vs $\omega^{-1/2}$ should give parallel straight lines at different applied potentials obtained in the mixed kinetic-diffusion-controlled region. The K-L plot (Fig. 10a and b) of Pd–PPy/C catalysts without and with methanol shows linearity and parallelism, confirming that ORR follows first-order kinetics with respect to molecular oxygen. Further, the plots do not pass through the origin, again indicating a mixed kinetic-diffusion-controlled mechanism.[32] The number of electrons involved in the ORR calculated using K-L equation works out to be 3.98 and 3.75 for without and with methanol, respectively. This confirms that oxygen reduction by the Pd–PPy/C catalyst occurs through a direct reduction of oxygen to water. The percentage of hydrogen peroxide generated at the ring at 0.4 V is calculated using the equation

$$\%\ H_2O_2 = \frac{2I_R/N}{I_D + (I_R/N)}$$

where I_D and I_R are the disk and ring currents, respectively, and N is the collection efficiency (0.24). In a typical calculation from the data in Fig. 9 (I_D = 0.81 mA, I_R = 0.0056 mA), the percentage of peroxide calculated for the Pd–PPy/C catalyst is 5.6%, which is very less even in the potential region where hydrogen peroxide formation is expected to be very high. Shao et al. showed a negligible extent of generation of hydrogen peroxide (ca. 4.1%) on the palladium monolayer and the palladium alloy electrocatalyst.[33]

In Fig. 11, log i_k is plotted vs potential in the mixed kinetic-diffusion controlled region that gives the Tafel plot. From the plot,

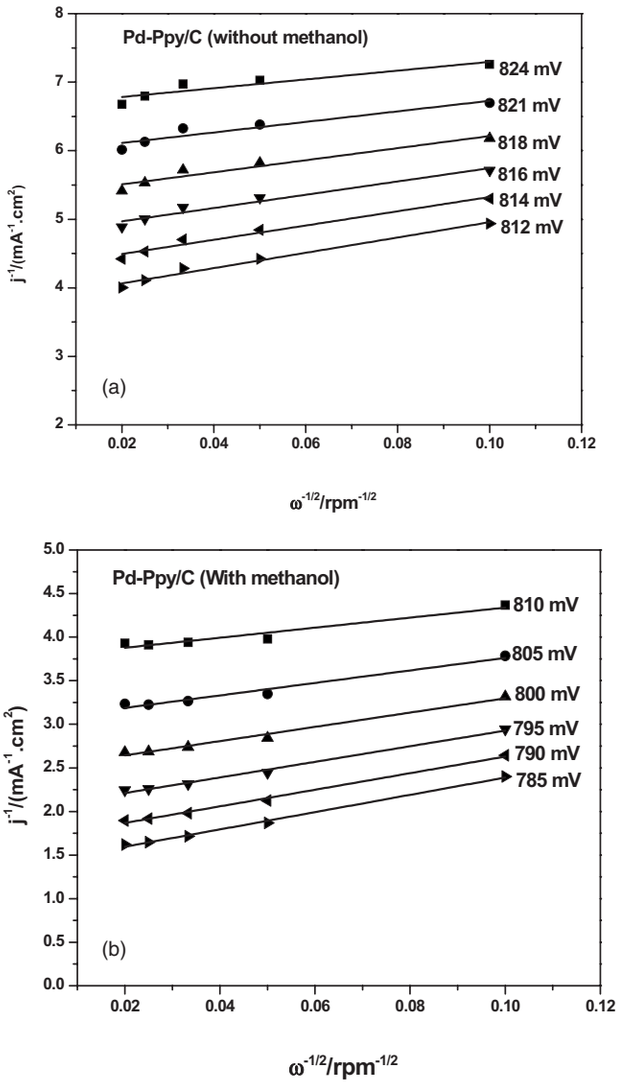

Figure 10. K-L plot for Pd–PPy/C: (a) without and (b) with 0.5 M methanol.

the Tafel slope is calculated. In the higher potential region, i.e., <0.80 V, the slope calculated is 60 mV dec^{-1} and it can be explained by a mechanism of oxygen reduction in which the reaction involves an initial fast charge-transfer step followed by a chemical step, which is the rate-determining step. The Tafel slope value remains unchanged in the presence of high methanol concentration, suggesting that methanol does not affect the kinetics of oxygen reduction on Pd–Ppy/C.

Conclusions

The Pd–PPy/C was prepared in two steps involving the preparation of PPy/C in the first step and the incorporation of Pd nanoparticles by reducing Pd^{2+} precursor salt using sodium borohydride in the second. The powder XRD pattern of Pd–PPy/C shows the formation of Pd metal nanoparticles in the fcc phase. Further, XPS analysis reveals an increase in d-band vacancy due to metal–polymer interaction, resulting in improved ORR kinetics. Cyclic voltammetric studies show that there is no change in the current corresponding to the reduction of Pd ion at ~0.68 V for several consecutive potential runs, indicating that the catalyst is stable in this electrochemical potential window. The thermal stability of Pd–PPy/C is good though it decomposes at ~50°C before the decomposition of PPy/C. Studies on the oxygen reduction activity using

Downloaded 19 Jan 2011 to 210.212.252.226. Redistribution subject to ECS license or copyright; see http://www.ecsdl.org/terms_use.jsp

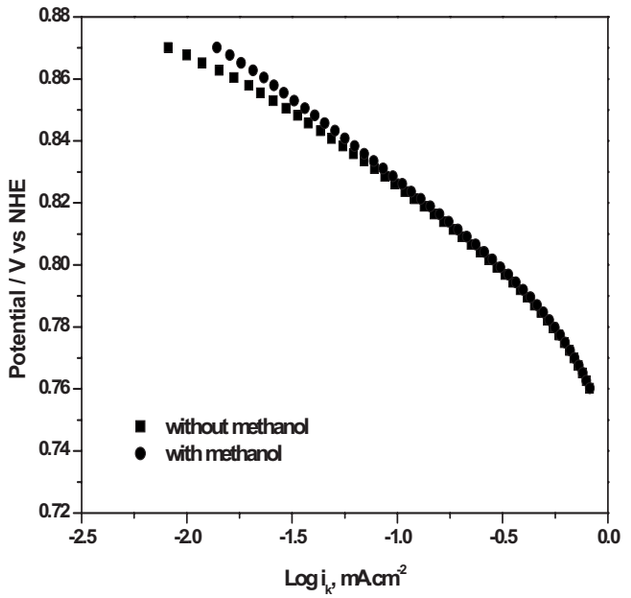

Figure 11. Tafel plot for Pd–PPy/C in presence and absence of methanol; rotation rate: 1600 rpm.

linear polarization measurements reveal that the $E_{1/2}$ value obtained from the polarization curve of ORR at 1600 rpm is 0.755 mV vs NHE. In comparison to Pt/C, some cathodic shift in $E_{1/2}$ of the polarization curve of ORR to ca. 60 mV was observed for Pd–PPy/C. In the presence of methanol, $E_{1/2}$ of the polarization curve of ORR on the Pd–PPy/C catalyst does not shift cathodically. However, this is not the case with Pt/C where >200 mV shift is observed. The ORR current on Pd–PPy/C with and without methanol remains unaffected, suggesting that the present catalyst is methanol-tolerant. The K-L plot of Pd–PPy/C catalysts shows linearity and parallelism, confirming that ORR follows first-order kinetics with respect to molecular oxygen. The number of electrons involved in ORR calculated using the K-L equation works out to be 3.98 and 3.75 for without and with methanol, respectively. This suggests that oxygen reduction on the Pd–PPy/C catalyst occurs through a direct reduction of oxygen to water. The generation of hydrogen peroxide at the ring (at 0.4 V) is very less and is $\sim 5\%$. The Tafel slope calculated for the Pd–PPy/C catalyst is 60 mV dec^{-1}, indicating that the initial fast charge-transfer step followed by a chemical step is the rate-determining step. Hence, Pd–PPy/C could be a suitable methanol-tolerant cathode material for oxygen reduction in DMFCs as it shows good stability, oxygen reduction activity, and methanol tolerance.

Acknowledgment

C.J. thanks CSIR for the Junior Research Fellowship. Authors thank the Department of Science & Technology, New Delhi for the financial assistance (SR/S1/PC-37/2004).

Central Electrochemical Research Institute assisted in meeting the publication costs of this article.

References

1. N. Alonso Vante, W. Jaegermann, H. Tributsch, W. Hoenle, and K. Yvon, *J. Am. Chem. Soc.*, **109**, 3251 (1987).
2. O. Solorza-Feria, K. Ellmer, M. Giersig, and N. Alonso-Vante, *Electrochim. Acta*, **39**, 1647 (1994).
3. K. Wiesener, D. Ohms, V. Neumann, and R. Franke, *Mater. Chem. Phys.*, **22**, 457 (1989).
4. G. Q. Sun, J. T. Wang, and R. F. Savinell, *J. Appl. Electrochem.*, **28**, 1087 (1998).
5. S. Gupta, D. Tryk, S. K. Zecevic, W. Aldred, D. Guo, and R. F. Savinell, *J. Appl. Electrochem.*, **28**, 673 (1998).
6. T. Toda, H. Igarashi, and M. Watanabe, *J. Electroanal. Chem.*, **460**, 258 (1999).
7. H. Yang, N. Alonso-Vante, J.-M. Léger, and C. Lamy, *J. Phys. Chem. B*, **108**, 1938 (2004).
8. E. Antolini, J. R. C. Salgado, and E. R. Gonzalez, *Appl. Catal., B*, **63**, 137 (2006).
9. Y. Xu, A. V. Ruban, and M. Mavrikakis, *J. Am. Chem. Soc.*, **126**, 4717 (2004).
10. A. K. Shukla, R. K. Raman, N. A. Choudhury, K. R. Priolkar, P. R. Sarode, S. Emura, and R. Kumashiro, *J. Electroanal. Chem.*, **563**, 181 (2004).
11. R. W. J. Scott, A. K. Datye, and R. M. Crooks, *J. Am. Chem. Soc.*, **125**, 3708 (2003).
12. M.-H. Shao, K. Sasaki, and R. R. Adzic, *J. Am. Chem. Soc.*, **128**, 3526 (2006).
13. C. Jeyabharathi, J. Mathiyarasu, and K. L. N. Phani, *Electrochim. Acta*, **54**, 448 (2008).
14. V. Raghuveer, A. Manthiram, and A. J. Bard, *J. Phys. Chem. B*, **109**, 22909 (2005).
15. J. Mathiyarasu and K. L. N. Phani, *J. Electrochem. Soc.*, **154**, B1100 (2007).
16. A. K. Shukla and R. K. Raman, *Annu. Rev. Mater. Sci.*, **33**, 155 (2003).
17. B. Rajesh, K. Ravindranathan Thampi, J.-M. Bonard, H. J. Mathieu, N. Xanthopoulos, and B. Viswanathan, *Chem. Commun. (Cambridge)*, **2003**, 2022.
18. G. Chen, Z. Wang, T. Yang, D. Huang, and D. Xia, *J. Phys. Chem. B*, **110**, 4863 (2006).
19. K.-M. Mangold, F. Meik, and K. Juttner, *Synth. Met.*, **144**, 221 (2004).
20. S. S. Kumar, C. S. Kumar, J. Mathiyarasu, and K. L. N. Phani, *Langmuir*, **23**, 3401 (2007).
21. C. Medard, M. Lefevre, J. P. Dodelet, F. Jaouen, and G. Lindbergh, *Electrochim. Acta*, **51**, 3202 (2006).
22. G. Faubert, G. Lalande, R. Cöte, D. Guay, J. P. Doddelet, L. T. Weng, P. Bertrand, and G. Denes, *Electrochim. Acta*, **41**, 1689 (1996).
23. R. Bashyam and P. Zelenay, *Nature (London)*, **443**, 63 (2006).
24. T. Ikeda, M. Boero, S.-F. Huang, K. Terakura, M. Oshima, and J. Ozaki, *J. Phys. Chem. C*, **112**, 14706 (2008).
25. J. Tsuji, *Palladium in Organic Synthesis*, Springer-Verlag, Berlin (2005).
26. O. Savadogo, K. Lee, K. Oishi, S. Mitsushima, N. Kamiya, and K.-I. Ota, *Electrochem. Commun.*, **6**, 105 (2004).
27. I. D. Kostas, A. G. Coutsolelos, G. Charalambidis, and A. Skondra, *Tetrahedron Lett.*, **48**, 6688 (2007).
28. C. Pu, W. Huang, K. L. Ley, and E. S. Smotkin, *J. Electrochem. Soc.*, **142**, L119 (1995).
29. L. Qiu, F. Liu, L. Zhao, W. Yang, and J. Yao, *Langmuir*, **22**, 4480 (2006).
30. A. J. Bard and L. R. Faulkner, *Electrochemical Methods*, 2nd ed., John Wiley & Sons, New York (2001).
31. H. Ye and R. M. Crooks, *J. Am. Chem. Soc.*, **129**, 3627 (2007).
32. G. Zhang and F. Yang, *Electrochim. Acta*, **52**, 6595 (2007).
33. M. H. Shao, T. Huang, P. Liu, J. Zhang, K. Sasaki, M. B. Vukmirovic, and R. R. Adzic, *Langmuir*, **22**, 10409 (2006).

Downloaded 19 Jan 2011 to 210.212.252.226. Redistribution subject to ECS license or copyright; see http://www.ecsdl.org/terms_use.jsp